$Rh(Phen)_2Phi^{3+}$ as a Shape-Selective Probe of Triple Helices†

Ai Ching Lim and Jacqueline K. Barton*

Division of Chemistry and Chemical Engineering, California Institute of Technology, Pasadena, California 91125

Received March 4, 1998; Revised Manuscript Received April 29, 1998

ABSTRACT: RNA pur•pur-pyr and pyr•pur-pyr (pur = purine, pyr = pyrimidine) triple helices consisting of a Watson−Crick base-paired 28mer hairpin duplex and a Hoogsteen base-paired purine or pyrimidine 12mer are targeted with photoactivated cleavage by the metal complex $Rh(phen)_2phi^{3+}$ (phen = phenanthroline, phi = 9,10-phenanthrenequinone diimine). The metal complex interacts with these triple helices in a structure-specific manner. Different cleavage patterns are seen with the pyr•pur-pyr and pur•pur-pyr motifs. Cleavage is seen on both of the Watson−Crick strands of the former motif and primarily on the purine Watson−Crick strand of the latter motif. Little cleavage is seen on the Hoogsteen strand for either motif. Importantly, the metal complex shows no detectable cleavage on the A-form RNA duplex in the absence of the third Hoogsteen strand. The cleavage patterns are consistent with an intercalated model for the metal complex in the triple helix. Similar cleavage is seen on DNA triple helices, but over a background of duplex cleavage. Targeting of synthetic RNA triple helices, but not duplex regions, by $Rh(phen)_2phi^{3+}$ provides a basis for the chemical probing of triply bonded sites in folded RNA molecules.

$Rh(phen)_2phi^{3+}$ is a unique site-selective probe for RNA structures that preferentially targets sites on folded RNA which are open or accessible for intercalative stacking from the major groove (*1*).

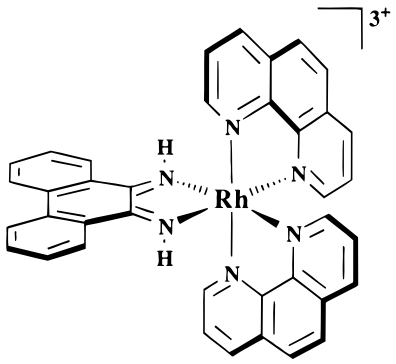

Δ-$Rh(phen)_2phi^{3+}$

These sites include major groove recognition sites for proteins (*2*) as well as sites of RNA tertiary interaction where triply bonded bases are arranged to permit stacking from the major groove. In studies which probed rhodium recognition sites on tRNAs and tRNA mutants (*3*), $Rh(phen)_2phi^{3+}$ was shown to target the triply bonded base segments which together establish the folded structure of the RNA. Metal complexes have been increasingly utilized as sensitive chemical probes of RNA structure and folding in solution (*4*, *5*). To characterize in more detail this recognition of triple bases by $Rh(phen)_2phi^{3+}$, and in so doing to explore the scope of the rhodium complex as a chemical probe for RNA tertiary structure, we have undertaken a study of rhodium complex reactions with synthetic RNA triple helices.

Triple helical structures were first described based upon fiber diffraction studies of the RNA polymers poly(U)•poly(A)-poly(U) (*6*). More recently, substantial interest has been focused on DNA and RNA triplexes in developing strategies for site-specific targeting for both genomic mapping (*7*) and therapeutic applications (*8*). Two triplex motifs have been elucidated, a purine•purine-pyrimidine (pur•pur-pyr) motif (*9*) and a pyrimidine•purine-pyrimidine (pyr•pur-pyr) motif (*6*). In the DNA pur•pur-pyr motif, the purine third strand was shown to bind in an antiparallel fashion to the purine strand of the Watson−Crick duplex in the major groove through Hoogsteen base-pairs (*9*). In the pyr•pur-pyr motif, the third strand binds in parallel to the purine Watson−Crick strand (*8*). Examples of both motifs have been identified also with RNA (*10*−*12*). Intramolecular DNA triple helices (termed H-DNA) have been observed in supercoiled plasmids (*13*) or may be formed from a single strand of chemically synthesized oligonucleotide (*14*). A crystal structure of parallel and antiparallel $(G•G-C)_2$ triple helix fragments formed from the overlap of overhanging DNA duplexes has been described (*15*). In both the parallel and antiparallel triplex fragments, the normal B-form DNA Watson−Crick components of the triplets are relatively unperturbed by the third strand.

A structural understanding of RNA triple helices is of interest in part because of the variety of triple base interactions which serve to direct the folding of complex RNA molecules (*4*). The base triples m^7G46-[G22-C13], G45-[m^2G10-C25], and A9-[A23-U12] help to generate and stabilize the structural core of $tRNA^{Phe}$ (*14*, *16*, *17*). Crystallographic data have established the presence of A•U-A and

† We are grateful to the National Institute of General Medical Sciences (GM33309) for their financial support of this research. Fellowship support was also provided by the Glaxo Research Co.

* Author to whom correspondence should be addressed.

S0006-2960(98)00509-1 CCC: $15.00 © 1998 American Chemical Society
Published on Web 06/05/1998

A•C-G triple bases in the P4-P6 domain of the *Tetrahymena* intron (*18*). These triples function in contributing to the tertiary folding of the intron. Chemical probes which preferentially target triply bonded bases in RNA molecules, therefore, could be powerfully applied as an aid in elucidating RNA tertiary structure and folding.

$Rh(phen)_2phi^{3+}$ recognizes RNA in a manner akin to its shape-selective recognition of DNA sites. $Rh(phen)_2phi^{3+}$ has been shown through NMR studies (*19*) and biophysical methods (*20*, *21*) to intercalate into duplex DNA from the major groove with high affinity. A high-resolution NMR structure of a related complex, Δ-α-Rh[(R,R)-$(Me_2Trien)_2$)]-phi^{3+} (Me_2Trien = 2,9-diamino-4,7-diazadecane), shows this major groove intercalation (*22*). Upon photoactivation, the rhodium complex promotes direct strand cleavage; product analysis is consistent with a photoreaction involving abstraction of the C3′-hydrogen atom directly by the photoexcited, intercalated phi ligand (*21*), and analogous studies on $tRNA^{Phe}$ (*1*) indicate equivalent products and efficiencies. The DNA sites selected for targeting by $Rh(phen)_2phi^{3+}$ correlate closely with sites identified crystallographically as being more open in the major groove, in particular those 5′-pyr-pyr-pur-3′ sites which show a large major groove opening due to a change in propeller twist (*23*). This preference for open major groove sites has been attributed to a high intercalative binding affinity of the phi ligand being modulated by significant steric clashes of the overhanging phenanthroline ligands with the base-paired helix; only at sites which are somewhat open in the major groove is stacking by the octahedral complex made facile.

There is precedence for intercalation into triple helices and triplex junctions both by synthetic metal complexes and by naturally occurring organic heterocycles (*24*−*27*). Several DNA-binding agents show greater affinity for triplex DNA than for duplex DNA and, in fact, can stabilize the triplex (*24*, *28*−*30*). Fe(II)•bleomycin is an example of a natural product which has been shown to preferentially cleave at duplex/triplex junctions (*31*).

$Rh(phen)_2phi^{3+}$ may be particularly useful in probing RNA tertiary structure because, despite binding through shape-selection to B-DNA sites, the complex neither binds nor cleaves A-form duplexes (*2*). This poor reactivity with RNA duplexes is consistent with the preferential intercalation of the complex in the major groove; since an A-form helix contains a narrow and deep major groove, intercalation by the octahedral complex is precluded (*1*−*3*). This is in contrast to the DNA analogue of $tRNA^{Phe}$, where cleavage is observed along the A-form stems (*32*). In the case of RNA triplexes, however, the third strand itself binds within the duplex major groove and this stacked array may provide an accessible platform for intercalation by the complex. Other tertiary interactions, bulges, and mismatches, which widen the major groove of RNA helices (*33*), may also permit access by the metal complex (*2*).

Here we focus specifically on this preferential recognition of RNA triplex structures by $Rh(phen)_2phi^{3+}$. We sought to characterize this interaction on a well-described triplex structure. Figure 1 illustrates the RNA triplex oligomers used as substrates in these studies. RNA or DNA pur•pur-pyr and pyr•pur-pyr triple helices consisting of a Watson−Crick base-paired 28mer duplex and a Hoogsteen base-paired purine or pyrimidine 12mer were formed by annealing DNA

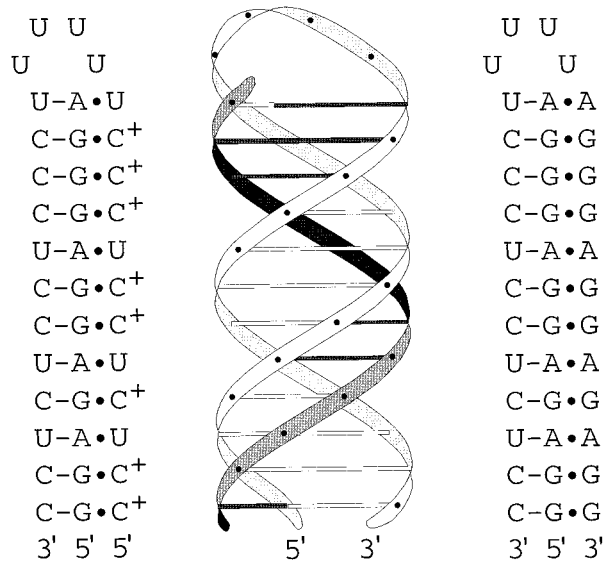

FIGURE 1: Schematic illustrations of the RNA triple helices used in this study. Triple helices were formed by annealing together a 28-mer RNA hairpin duplex 5′-GGAGAGGAGGGAUUUUUC-CCUCCUCUCC-3′) with either a 12-mer purine strand (5′-AGGGAGGAGAGG-3′) or a 12-mer pyrimidine (5′-CCUCUC-CUCCCU-3′) strand.

or RNA 28mer hairpin duplexes with the corresponding RNA or DNA purine or pyrimidine 12mers of defined sequence. The RNA and DNA pyr•pur-pyr synthetic triple helices have already been characterized thermodynamically (*34*, *35*). $Rh(phen)_2phi^{3+}$ cleavage may then be compared and contrasted to both the RNA and DNA hairpin duplexes and their corresponding triplexes.

Here we find that the metal complex interacts with these triple helices in a structure-specific manner. Different cleavage patterns are seen with the pyr•pur-pyr and pur•pur-pyr motifs. Cleavage is seen on both Watson−Crick strands of the former motif and primarily on the purine Watson−Crick strand of the latter motif. Little cleavage is seen on the Hoogsteen strand for either motif. Importantly, the metal complex shows no detectable cleavage on the A-form RNA duplex in the absence of a third strand. The cleavage patterns are consistent with an intercalated model for the metal complex in the triple helix. Similar cleavage patterns are seen on DNA triple helices, but over a background of duplex cleavage. Targeting of synthetic RNA triple helices but not duplex regions by $Rh(phen)_2phi^{3+}$ therefore provides a basis for the chemical probing of triply bonded sites in folded RNA molecules.

EXPERIMENTAL METHODS

RNA Oligomers. RNA oligonucleotides were chemically synthesized on a 1 μmol scale on an Applied Biosystems 392 DNA/RNA synthesizer using phosphoramidite chemistry. Oligomers were desalted and failure sequences removed using an oligonucleotide purification column from Applied Biosystems. Extinction coefficients at 260 nm were 10200, 7300, and 8800 M^{-1} cm^{-1} $nucleotide^{-1}$ based on nucleotide composition for the purine 12mer, the pyrimidine 12mer, and the 28mer, respectively. Oligomers were 3′-end-labeled with cytidine 3′,5′-[5′-^{32}P]bisphosphate using T4 RNA ligase (*36*) or 5′-end-labeled with [γ-^{32}P]ATP using T4 polynucleotide kinase. Samples were then gel purified on a 10%

denaturing polyacrylamide gel, located by autoradiography, excised, and eluted from the gel slice in 45 mM Tris-HCl, 45 mM boric acid, 1.25 mM EDTA, pH 8.0. The eluted RNA oligomers were ethanol-precipitated twice and stored frozen in 10 mM Tris-HCl, pH 7.5.

DNA Oligomers. DNA analogues of the RNA strands were chemically synthesized on a 1 μmol scale on an Applied Biosystems 392 DNA/RNA synthesizer using phosphoramidite chemistry. Oligonucleotides were purified twice by HPLC, first with the dimethoxytrityl (DMT) group on and subsequently with the DMT group off using a C_{18} column (Dynamax). The oligonucleotides were further purified on a 10% denaturing polyacrylamide gel, located by UV shadowing, excised, and eluted from the gel in 45 mM Tris-HCl, 45 mM boric acid, 1.25 mM EDTA, pH 8.0. The eluted DNA oligomers were concentrated by a Centricon 10 (Amicon) device, desalted by washing twice with water, and stored in 10 mM Tris-HCl, pH 7.5. Extinction coefficients at 260 nm were 9300, 7300, and 8300 M^{-1} cm^{-1} nucleotide^{-1} based on nucleotide composition for the purine 12mer, the pyrimidine 12mer, and the 28mer, respectively. The oligomers were then 3′-end-labeled with [α-^{32}P]ddATP using terminal deoxytransferase or 5′-end-labeled with [γ-^{32}P]ATP using T4 polynucleotide kinase. The labeled materials were gel-purified by the same method as for RNA oligomers and stored frozen in 10 mM Tris-HCl, pH 7.5.

Triplex Formation. Gel retardation assays were employed to establish triplex formation. In separate experiments, either the hairpin or third strand was radioactively labeled, and conditions for retardation relative to the double-stranded or single-strand controls, respectively, were determined. Duplex alone or duplex bound to either the purine or pyrimidine 12mer to a final total concentration of 100 μM in nucleotides were renatured by heating to 65 °C for 1 min in 10 mM Tris-HCl, 10 mM $MgCl_2$, 1 mM spermidine, pH 5.5, and slowly cooling to 4 °C. The samples were then allowed to stand at 4 °C for 4−12 h. Samples were then loaded onto a 10 or 20% polyacrylamide gel at 4 °C which had been prepared with 50 mM sodium acetate, 1 mM EDTA, pH 5.5 or 7.0. Samples were electrophoresed at low voltage at 4 °C before being visualized by autoradiography.

Cleavage Reactions. [Rh(phen)$_2$phi]Cl_3 was synthesized as described previously (*20*). All metal stock solutions were freshly prepared in either ethanol or 10 mM Tris-HCl, pH 7.5. The end-labeled oligomers, with either carrier oligomer or $tRNA^{Phe}$ (Boehringer Mannheim) at a final concentration of 100 μM in nucleotides, were renatured by heating to 65 °C for 1 min in 10 mM Tris-HCl, 10 mM $MgCl_2$, 1 mM spermidine, pH 5.5 or 7.0, and slowly cooled to 4 °C. At this temperature, 2.5−10 μM metal complex (freshly diluted in H_2O) was then added. The 20 μL mixture was incubated between 5 min and 12 h at 4 °C and was then irradiated at 365 or 313 nm at ambient temperature or on ice using a 1000-W Hg/Xe lamp and monochromator (Oriel model 77250). The reaction mixtures were ethanol precipitated and washed at least three times with ethanol to remove buffer salts, and then dried on a SpeedVac Concentrator (Savant).

RNase Digestions. Annealed duplexes and triplexes, with carrier oligomer to a final concentration of 28 μM in nucleotides in buffer, were prepared in the manner described for the metal cleavage reactions and incubated at 4 °C. One to five units of either RNase *Physarum polycephalum* (*Phy*M) or RNase *Bacillus cereus* (*Bc*) (Pharmacia) was added, and the samples were incubated for 15−70 min at 4 °C before being ethanol precipitated and dried, or quenched with denaturing loading dye.

Sequencing Gels. The cleavage products were analyzed on 20% polyacrylamide−8M urea gels and viewed by autoradiography. The full-length RNA oligomers and cleavage products were identified by coelectrophoresing with $Ru(phen)_3^{2+}$ (G-specific) reactions (*1*), diethyl pyrocarbonate (DEPC) (A-specific) and hydrazine (U-specific) reactions (*37*), and the full-length DNA oligomers and cleavage products by piperidine formate (A+G-specific), hydrazine hydrate (C+T-specific), dimethyl sulfate (G-specific), or hydrazine/NaCl (C-specific) Maxam Gilbert reactions (*38*). The fragments produced by the metal complex cleavage possess 3′ and 5′ phosphate termini, and thus may be directly compared with the chemical sequencing lanes (*1*).

Factors Affecting Triplex Formation and Cleavage. The annealing temperature of the triplex was critical, as incubation at room temperature alone was not sufficient to promote formation of the triple helix. It has been reported (*39*) based on gel-shift data that a similar RNA pur•pur-pyr motif could not be formed despite the fact that the DNA analogue folded properly. The addition of spermidine and incubation at cooler temperatures in the experiments reported here clearly aided the formation of the pur•pur-pyr motif. Best results were obtained when duplex and third strand were allowed to anneal and slowly cooled from 65 to 4 °C. The incubation time of the oligomers was also important. Samples were incubated from 8 to 24 h at 4 °C; longer incubation did not produce more cleavage. Based on gel retardation assays, the pur•pur-pyr motif was formed in greater yield than the pyr•pur-pyr motif. Once the triplex was annealed, the metal complex could be added and photolyzed immediately (5 min) or after as much as 12 h with no equal cleavage efficiency.

Melting Studies of RNA Duplexes and Triplexes. RNA duplex and triplex melting temperatures were measured on a Beckman DU 7400 UV−vis spectrophotometer equipped with a 6 cell melting temperature unit. The concentration of nucleic acid strands was kept constant at 1.33 μM ends, or the total RNA nucleotide concentration was kept constant at 50 μM. Solutions were prepared in 10 mM Tris-HCl, 10 mM $MgCl_2$, and 1 mM spermidine at pH 5.5, and incubated at 90 °C for 5 min. The samples were then annealed from 90 °C to 4 °C at 0.5 deg/min intervals, halted at 4 °C for 60 min, then heated to 90 °C again at 0.5 deg/min intervals. The absorption was monitored at 260 nm.

The melting temperature of the RNA duplex was found to be 79 ± 1 °C. The melting temperature curves of the triplexes also had a single inflection point, and it was not possible to distinguish when the third strand melted. However, the addition of the third strand raised the melting temperature of the duplex. The melting temperature of the pur•pur-pyr motif was found to be 85 ± 1 °C, while that of the pyr•pur-pyr motif was found to be 84 ± 3 °C. Thus, even though the transition where the third strand melts is not observed, the addition of the third strand does appear to stabilize the duplex. It was not possible to do the melting studies of the RNA oligomers in the presence of metal complex, as the melting temperatures were too high.

*Gel Retardation Assay for Triplex Formation***.** The RNA pur•pur-pyr triplex was found to be substantially retarded

in its mobility compared to the labeled single RNA homopurine strand, and conditions for triplex formation established with this assay were applied in photocleavage experiments. The analogous RNA pyr•pur-pyr triple helices, although substantially formed, were formed in variable yield compared to the pur•pur-pyr helices. These retardation assays were therefore used as a routine screening assay before photocleavage reactions. The analogous DNA pur•pur-pyr and pyr•pur-pyr helices could be formed using these same conditions.

Quantitation. Quantitation was accomplished using photostimulable storage phosphorimaging Kodak screen S0230 from Molecular Dynamics. A Molecular Dynamics 400S PhosphorImager was used to scan the screens, and Imagequant version 3.3 was used to analyze the data.

RESULTS

Recognition of RNA Pur•Pur-Pyr Triple Helices by Rh(phen)$_2$phi^{3+}. Figure 2 illustrates the shape-selective targeting of RNA pur•pur-pyr triple helices by Rh(phen)$_2$phi^{3+}. In the experiment shown, the 3′-^{32}P-end-labeled hairpin RNA was incubated in the presence and absence of the purine strand and then tested for photocleavage by Rh(phen)$_2$phi^{3+}. The rhodium complex shows no detectable cleavage of the RNA hairpin duplex. Rh(phen)$_2$phi^{3+} does not appear to intercalate into an A-form helix. This observation is fully consistent with earlier studies of tRNA^{Phe} and other folded RNAs (*2*). However, upon the addition of the third RNA strand with the consequent formation of the pur•pur-pyr triplex, distinct cleavage becomes evident at each purine position of the duplex strand as well as throughout the tetrauridine loop of the hairpin.

Cleaved fragments are found to comigrate with 5′-phosphate products consistent with the rhodium photocleavage chemistry (*21*). Also consistent with the photochemistry (*40*), reduced but detectable cleavage is observed on the triplex at pH 5.5. Experiments were also conducted using the 5′-^{32}P-end-labeled hairpin strand, and equivalent results were obtained; fragments comigrated with 3′-phosphate products. Relatively sequence-neutral cleavage was observed across the double-stranded purine region and the tetrauridine hairpin loop in the triplex, but not in the hairpin duplex alone, as schematically illustrated in Figure 3. Rh(phen)$_2$phi^{3+}, therefore, is found to bind preferentially and, upon photoactivation, to promote cleavage throughout the triple helical region.

Importantly, the observation of cleavage across the hairpin loop of the triplex but not within the hairpin of the duplex must also indicate a conformational change in the loop which is a consequence of triplex formation. Triplex formation therefore imparts hypersensitivity of the loop region to the rhodium complex. In earlier studies of folded RNAs (*2*), Rh(phen)$_2$phi^{3+} was found to promote cleavage within loops which were stacked and structured. The result here suggests that formation of the triplex imparts structure to the loop, perhaps in exerting some torque onto the loop region which more tightly stacks the bases, promoting binding and cleavage by the metal complex.

Parallel photocleavage experiments with rhodium complexes were conducted using a 3′-^{32}P-end-labeled purine strand and unlabeled hairpin duplex. Under comparable

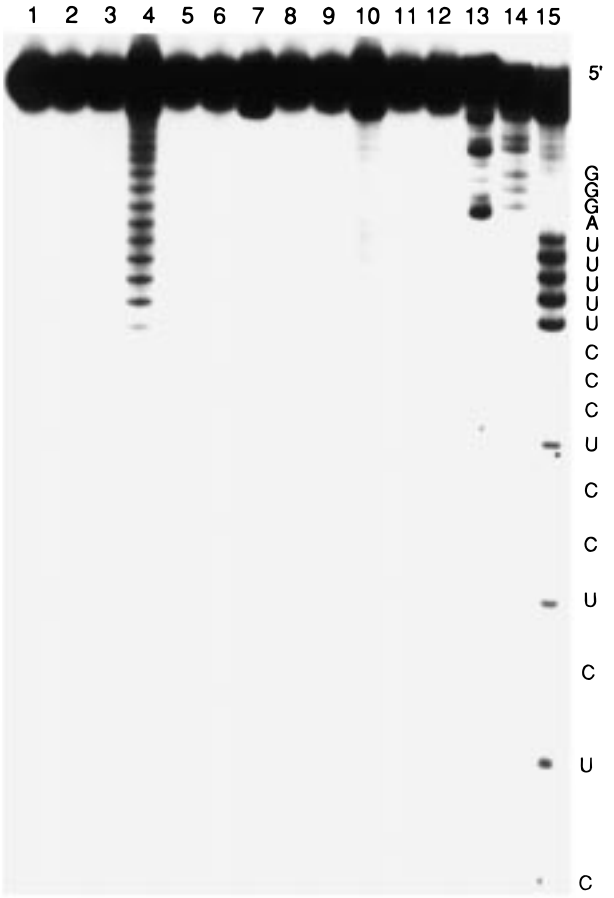

FIGURE 2: Autoradiogram showing cleavage of 3′-^{32}P-labeled RNA duplex (lanes 1−3, 7−9) and RNA pur•pur-pyr triplex (lanes 4−6, 10−12) by Rh(phen)$_2$phi^{3+} in 10 mM Tris-HCl, 10 mM $MgCl_2$, 1 mM spermidine, pH 7.0 (lanes 1−6) and pH 5.5 (lanes 7−12). Lanes 1 and 7: labeled RNA duplex after incubation with 10 μM Rh(phen)$_2$phi^{3+} and irradiation for 10 min at 313 nm. Lanes 2 and 8: labeled RNA duplex after incubation with 10 μM Rh(phen)$_2$phi^{3+}. Lanes 3 and 9: labeled RNA duplex after irradiation for 10 min at 313 nm. Lanes 4 and 10: cleaved RNA pur•pur-pyr triplex after incubation with 10 μM Rh(phen)$_2$phi^{3+} and irradiation for 10 min at 313 nm. Lanes 5 and 11: labeled RNA pur•pur-pyr triplex after incubation with 10 μM Rh(phen)$_2$phi^{3+}. Lanes 6 and 12: labeled RNA pur•pur-pyr triplex after irradiation for 10 min at 313 nm. Lanes 13, 14, and 15: A-, G-, and U-specific reactions on the labeled RNA duplex, respectively.

conditions, little cleavage is detected on the purine strand, both in the absence and presence of the hairpin duplex. At higher concentrations of metal complex and with longer irradiation times, some background cleavage on the labeled single strand may be detected, but no increase in cleavage intensity is observed upon addition of duplex. Consistent with earlier studies, Rh(phen)$_2$phi^{3+}, then, does not promote significant cleavage of single-stranded RNA. Also, although the rhodium complex binds and cleaves the triplex along the Watson−Crick purine strand, no significant cleavage is found on the third purine strand.

Recognition of RNA Pyr•Pur-Pyr Triple Helices by Rh(phen)$_2$phi^{3+}. Figure 4 shows an autoradiogram of a gel which demonstrates the shape-selective targeting also of pyr•pur-pyr triple helices by Rh(phen)$_2$phi^{3+}. Again, no significant cleavage is seen in the RNA duplex without the addition of the third strand. In the presence of the third pyrimidine strand, and in contrast to the pur•pur-pyr motif, cleavage by Rh(phen)$_2$phi^{3+} is observed across both the

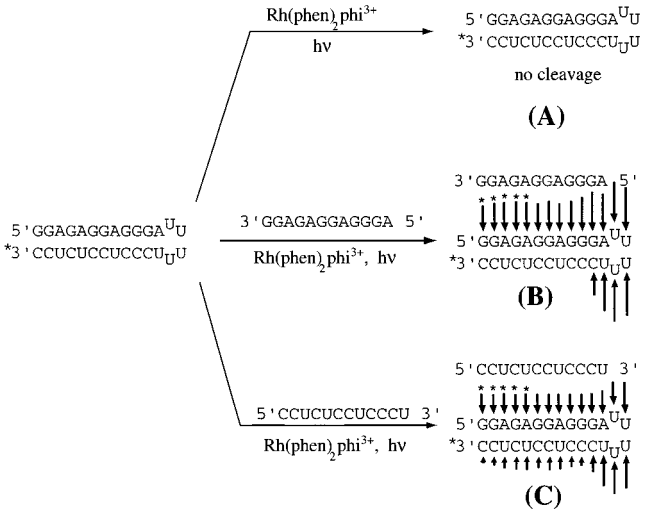

FIGURE 3: Schematic illustration of light-induced $Rh(phen)_2phi^{3+}$ cleavage on the RNA duplex (**A**), RNA pur•pur-pyr triplex (**B**), and RNA pyr•pur-pyr triplex (**C**). Cleavage intensities on each motif (as determined by integration using ImageQuant) are depicted by the size of the arrows. Cleavage intensities between different motifs should not be compared, due to the different yields of formation for each motif. Arrows with asterisks are approximations only, as quantitation was difficult due to the closeness of the bands. No cleavage is evident on the duplex strand alone, while relatively sequence-neutral cleavage is seen on the purine side of the Watson−Crick duplex on the pur•pur-pyr motif. Cleavage is seen throughout the Watson−Crick duplex on the pyr•pur-pyr motif.

purine and pyrimidine strands of the Watson−Crick duplex. Phosphorimager quantitation with baseline correction showed a somewhat greater amount of cleavage on the purine side of the duplex than on the pyrimidine side. This observation is to be contrasted to those with the pur•pur-pyr motif, in which no cleavage was apparent on the pyrimidine side of the hairpin duplex.

As in the pur•pur-pyr motif, cleavage by the rhodium complex is also observed across the hairpin loop in the triplex but not the duplex. Here, cleavage is in fact more intense within the loop region than across the triplex. This targeting of the loop supports the idea that triplex formation with either motif leads to a conformational change or torque in the flanking loop region, which increases the association with the rhodium complex. No significant cleavage is evident on the third pyrimidine strand of the triplex in experiments using 3′-^{32}P-end-labeled pyrimidine strand, a finding similar to that in the pur•pur-pyr motif case.

Cleavage by $Rh(phen)_2phi^{3+}$ of the pyr•pur-pyr triplex is seen to depend on rhodium concentration, as well as time and wavelength for irradiation in a manner consistent with the photoreaction. Here, triplex cleavage is observed only at low pH (5.5) under conditions which stabilize the pyr•pur-pyr triplex (*41*). The photocleavage efficiency of $Rh(phen)_2phi^{3+}$ is, however, reduced at lower pH (*40*). Thus a quantitative comparison of the various efficiencies of rhodium complex cleavage of the pyr•pur-pyr motif versus the pur•pur-pyr motif is made difficult because of the lower yield of the pyr•pur-pyr motif and the necessity for low pH conditions. Figure 3 summarizes in a histogram format the cleavage results on the RNA hairpin duplex and two RNA triplexes.

Dependence of Cleavage on Carrier and Salt Concentrations. Experiments varying the carrier oligonucleotide were

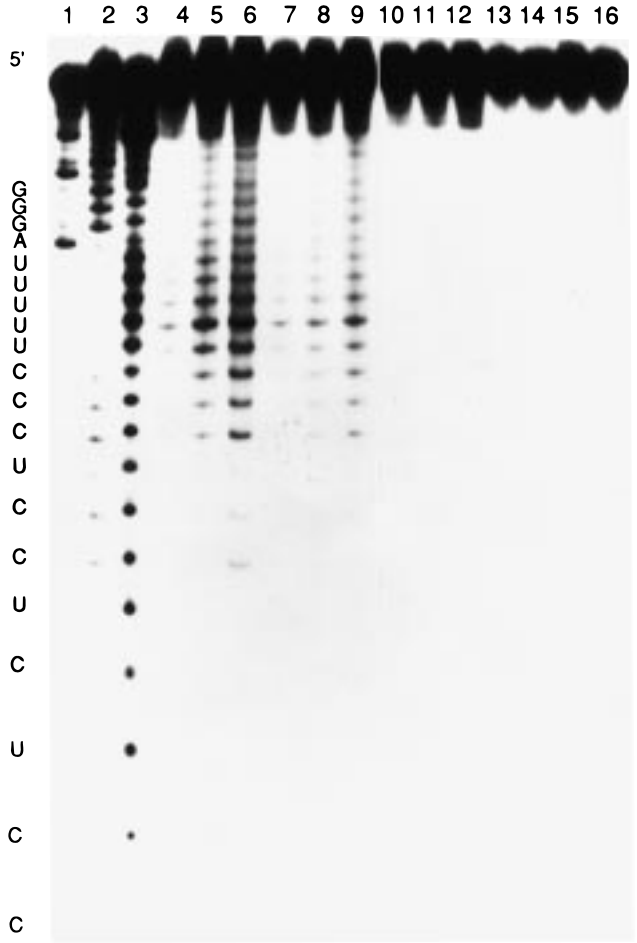

FIGURE 4: Autoradiogram showing cleavage of 3′-^{32}P-labeled RNA duplex (lanes 13−16) and pyr•pur-pyr triplex (lanes 4−12) by $Rh(phen)_2phi^{3+}$ in 10 mM Tris-HCl, 10 mM $MgCl_2$, 1 mM spermidine, pH 5.5. Lanes 1−3: A-, G-, and U- specific reactions, respectively. Lanes 4−6: cleaved RNA pyr•pur-pyr triplex, after incubation with 10 μM $Rh(phen)_2phi^{3+}$ and irradiation for 5, 10, and 20 min, respectively, at 313 nm. Lanes 7−9: cleaved RNA pyr•pur-pyr triplex, after incubation with 5 μM $Rh(phen)_2phi^{3+}$ and irradiation for 5, 10, and 20 min, respectively at 313 nm. Lanes 10−12: cleaved RNA pyr•pur-pyr triplex, after incubation with 1 μM $Rh(phen)_2phi^{3+}$ and irradiation for 5, 10, and 20 min, respectively, at 313 nm. Lane 13: labeled RNA duplex after incubation with 1 μM $Rh(phen)_2phi^{3+}$ and irradiation for 20 min at 313 nm. Lane 14: labeled RNA duplex after incubation with 10 μM $Rh(phen)_2phi^{3+}$ and irradiation for 20 min at 313 nm. Lane 15: labeled RNA duplex with 10 μM $Rh(phen)_2phi^{3+}$, but without irradiation. Lane 16: labeled RNA duplex upon irradiation for 10 min at 313 nm.

carried out on the pur•pur-pyr triplex. The same cleavage pattern and cleavage intensity were seen regardless of whether carrier oligonucleotide or $tRNA^{Phe}$ is used. This suggests that $Rh(phen)_2phi^{3+}$ has the same or greater binding affinity for the triplex as for $tRNA^{Phe}$, which is at least 3.5×10^5 M^{-1} (*42*). In addition, very little dependence of cleavage on carrier oligonucleotide concentration was observed when the concentration of carrier was varied from as little as 14 μM to 100 μM nucleotide, which is expected as the thermal stability of a triplex is Na^+-dependent, but nearly independent of triplex concentration (*43*). In this system, triplex formation was better stabilized by Mg^{2+} than by Na^+, and only a modest range of Na^+ concentrations were sampled (5−100 mM); cleavage by $Rh(phen)_2phi^{3+}$ did not show a large degree of Na^+ dependence through this range. How-

ever, there was a dependence on polycations such as Mg^{2+} and spermidine, which promoted triplex formation and hence cleavage. When a competition experiment was carried out with the analogous DNA oligomers as carrier, it was found that the intensity of cleavage in the RNA triplex was undiminished. This again points to the particularly high affinity for the RNA triplex substrate by $Rh(phen)_2phi^{3+}$.

Cleavage of RNA Triple Helices with RNases. Results of cleavage by the synthetic metal complex may also be compared to cleavage results using enzymatic probes for RNA single strands. Both RNase *Phy*M (A-, G-, and U-specific) and RNase *Bc* (C- and U-specific) (*44*) produce cleavage primarily in the loop region of the hairpin, both alone and when bound to a third strand. As illustrated in Figure 5, the purine triplex motif confers a degree of protection on the exposed loop region *Bc* digestion, compared to that for the duplex. It is also interesting to note that the addition of the purine third strand promotes RNase cleavage on the purine side of the duplex, even though this RNase is not specific for purines. This cleavage could be due to the widening of the major groove of the duplex to accommodate the third strand, thus rendering it more susceptible to nucleases. We find that there is 85%, 53%, and 86% digestion of the parent RNA band respectively in the duplex, pur•pur-pyr and pyr•pur-pyr lanes with identical amounts of RNase *Bc* and digestion time.

Similar results are observed when the RNA motifs are digested with RNase *PhyM* (Figure 5). Again, RNase digestion of the loop region is decreased in the purine triplex compared to the duplex. Cleavage is also apparent on the purine side of the duplex when bound to the purine third strand, as opposed to the lack of cleavage in the duplex alone. Cleavage in the loop region of the duplex in the pyr•pur-pyr triplex motif is also diminished compared to the duplex alone, but less so than with the pur•pur-pyr triplex motif.

This differential cleavage of the hairpin loops in the duplex compared to the triplex form complements the results seen with $Rh(phen)_2phi^{3+}$. Thus, a triplex-induced conformational change in the loop region can be detected by both metal complex and RNase cleavage.

Recognition of DNA Triple Helices by Rh(phen)$_2$phi^{3+}. Rhodium-promoted cleavage was also examined on the analogous DNA triplexes formed by annealing together the DNA hairpin duplex with either a pyrimidine or purine DNA third strand. When the labeled DNA duplex alone is irradiated in the presence of metal complex, one observes the expected cleavage by $Rh(phen)_2phi^{3+}$ of B-form DNA due to its open major groove (*21*), as seen in Figure 6. Cleavage of the pyrimidine strand of the duplex is, however, seen to be somewhat greater than of the purine strand. Upon addition of the purine third strand, however, there is a significant loss of cleavage on the pyrimidine side of the hairpin; cleavage on the purine side of the hairpin does not change substantially. Interestingly, addition of the pyrimidine third strand, in contrast, leads to a substantial reduction in cleavage on the purine side of the hairpin strand, while cleavage on the pyrimidine side remains largely intact. As on the RNA oligomers, there is a background of nonspecific cleavage at high metal complex and irradiation times on the labeled single-stranded oligomers alone, with no change upon addition of the unlabeled hairpin duplex. These results are shown in Figure 6 and schematically illustrated in histogram form in Figure 7. These data resemble those obtained with the RNA triple helices. However, the result is less striking in comparing the duplex to triplexes owing to the high level of cleavage obtained on the DNA duplex alone. This is consistent with the normal recognition of the DNA B-form helix by $Rh(phen)_2phi^{3+}$ (*21*).

DISCUSSION

Recognition of RNA Triple Helices by Rhodium Complexes. The results described here indicate that $Rh(phen)_2phi^{3+}$ targets RNA triple helices under conditions where significant cleavage is not evident on corresponding RNA duplexes. This recognition is structure-specific rather than sequence-specific, as cleavage across the triple helical segment in a sequence-neutral fashion is observed. $Rh(phen)_2phi^{3+}$ generally appears to be sensitive to the width of the major groove, and less so to the bases themselves. Hence, $Rh(phen)_2phi^{3+}$ may be particularly useful in probing RNA tertiary structures where the width of the major groove has been increased.

DNA triple helices are also targeted by the rhodium complex. In this case, however, cleavage is also evident on B-DNA duplexes, and $Rh(phen)_2phi^{3+}$ is thus less useful as a probe. The Watson−Crick base-paired duplex in the DNA triplex is considered to be still essentially B-form in nature (*15*), and the rhodium complex is not sensitive to this lack of change in the width of the major groove.

We attribute the novel RNA recognition characteristics of $Rh(phen)_2phi^{3+}$ to its shape-selective intercalation in the major groove. In this model, a triple helix could provide a platform of bases for intercalative stacking by the complex from the major groove side; such an intercalative interaction is sterically accessible. In contrast, an A-form duplex would provide a poor target for intercalative stacking from the major groove side, since, in an A-form helix, the major groove is narrowed and deepened, so that the phi complexes cannot access the base-pairs. Modeling shows that while the third strand of a helix fills the major groove, intercalation between base steps is still sterically facile and would permit greater stacking of the intercalating ligand at a base step.

RNA triple helices of both motifs, pur•pur-pyr and pyr•pur-pyr, are targeted by $Rh(phen)_2phi^{3+}$, although the cleavage characteristics across the triple helices differ for the two motifs. For the pur•pur-pyr motif, cleavage is observed preferentially on the purine Watson−Crick strand, while in the pyr•pur-pyr motif, cleavage is observed on both Watson−Crick strands. The difference in cleavage pattern across the triplex between the two motifs might be viewed in the context of a simple intercalation model. Given the dearth of direct structural data concerning intercalation into a triple helix, any modeling must be only very conservatively approached. We therefore restrict our consideration only to stacking directions, not detailed three-dimensional views. Several full-dimensional models were explored using both enantiomers of the metal complex in developing these schematic views, however.

Figure 8 illustrates the triplex hydrogen bonding pattern considered for the two motifs as well as the direction of intercalation suggested by the cleavage results. The differential cleavage on the two motifs by the metallointercalator might best be understood in terms of how the phi intercalator

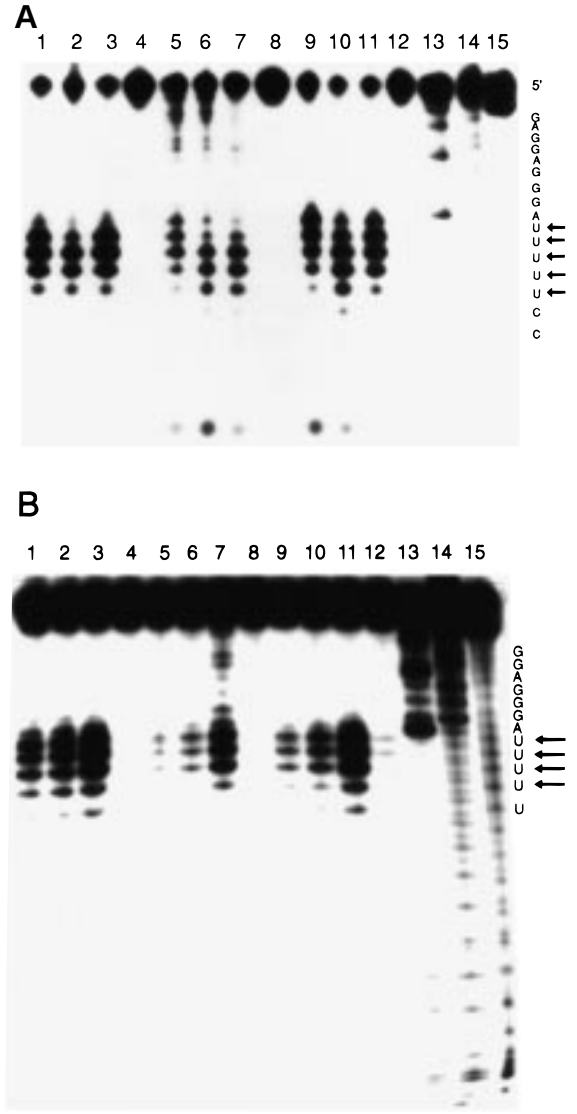

FIGURE 5: Autoradiogram showing cleavage of 3′-^{32}P-labeled RNA duplex (lanes 1−4), pur•pur-pyr triplex (lanes 5−8), and pyr•pur-pyr triplex (lanes 9−12) by (**A**) RNase *Bc* and (B) RNase *PhyM* in 10 mM Tris-HCl, 10 mM $MgCl_2$, 1 mM spermidine, pH 5.5. In (**A**): Lanes 1 and 2: cleaved RNA duplex, after incubation with 2 units RNase *Bc* for 15 and 60 min, respectively. Lane 3: cleaved RNA duplex, after incubation with 1 unit RNase *Bc* for 70 min. Lane 4: labeled RNA duplex. Lanes 5 and 6: cleaved RNA pur•pur-pyr triplex, after incubation with 2 units RNase *Bc* for 15 and 60 min, respectively. Lane 7: cleaved pur•pur-pyr RNA triplex, after incubation with 1 unit RNase *Bc* for 70 min. Lane 8: labeled RNA pur•pur-pyr triplex. Lanes 9 and 10: cleaved RNA pyr•pur-pyr triplex, after incubation with 2 units RNase *Bc* for 15 and 60 min, respectively. Lane 11: labeled RNA pyr•pur-pyr triplex, after incubation with 1 unit RNase *Bc* for 70 min. Lane 12: labeled RNA pyr•pur-pyr triplex. Lanes 13, 14, and 15: A-, G-, and U-specific reactions on the labeled RNA duplex, respectively. In (**B**): Lanes 1 and 2: cleaved RNA duplex, after incubation with 1 unit RNase *PhyM* for 15 and 60 min, respectively. Lane 3: cleaved RNA duplex, after incubation with 5 units RNase *PhyM* for 60 min. Lane 4: labeled RNA duplex. Lanes 5 and 6: cleaved RNA pur•pur-pyr triplex, after incubation with 1 unit RNase *PhyM* for 15 and 60 min, respectively. Lane 7: cleaved RNA pur•pur-pyr triplex, after incubation with 5 units RNase *PhyM* for 60 min. Lane 8: labeled RNA pur•pur-pyr triplex. Lanes 9 and 10: cleaved RNA pyr•pur-pyr triplex, after incubation with 1 unit RNase *PhyM* for 15 and 60 min, respectively. Lane 11: labeled RNA pyr•pur-pyr triplex, after incubation with 5 units RNase *PhyM* for 60 min. Lane 12: labeled RNA pyr•pur-pyr triplex. Lanes 13, 14, and 15: A-, G-, and U-specific reactions on the labeled RNA duplex, respectively.

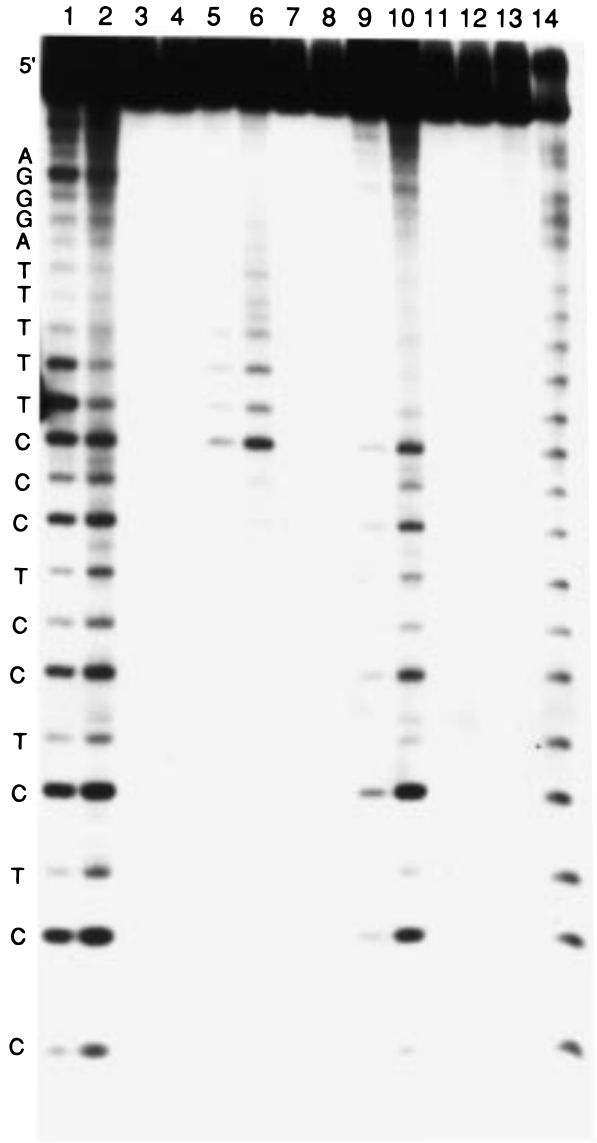

FIGURE 6: Autoradiogram showing cleavage of 3′-^{32}P-labeled DNA duplex (lanes 1−4), pur•pur-pyr triplex (lanes 5−8), and pyr•pur-pyr triplex (lanes 9−12) by $Rh(phen)_2phi^{3+}$ in 10 mM Tris-HCl, 10 mM $MgCl_2$, 1 mM spermidine, pH 5.5. Lanes 1 and 2: cleaved DNA duplex, after incubation with 10 μM $Rh(phen)_2phi^{3+}$ and irradiation for 2 and 10, min at 313 nm, respectively. Lane 3: labeled DNA duplex with 10 μM $Rh(phen)_2phi^{3+}$, but without irradiation. Lane 4: labeled DNA duplex upon irradiation for 10 min at 313 nm. Lanes 5 and 6: cleaved DNA pur•pur-pyr triplex, after incubation with 10 μM $Rh(phen)_2phi^{3+}$ and irradiation for 2 and 10 min at 313 nm, respectively. Lane 7: labeled DNA pur•pur-pyr triplex with 10 μM $Rh(phen)_2phi^{3+}$, but without irradiation. Lane 8: labeled DNA pur•pur-pyr triplex upon irradiation for 10 min at 313 nm. Lanes 9 and 10: cleaved DNA pyr•pur-pyr triplex, after incubation with 10 μM $Rh(phen)_2phi^{3+}$ and irradiation for 2 and 10 min at 313 nm, respectively. Lane 11: labeled DNA pyr•pur-pyr triplex with 10 μM $Rh(phen)_2phi^{3+}$, but without irradiation. Lane 12: labeled DNA pyr•pur-pyr triplex upon irradiation for 10 min at 313 nm. Lanes 13 and 14: A+G and C+T Maxam Gilbert sequencing reactions, respectively.

stacks on the bases. In the pur•pur-pyr motif, the four aromatic rings of the two purine bases (on the Hoogsteen strand and Watson−Crick base-pair) would provide a larger aromatic surface for stacking by the phi ligand than the three aromatic rings of the Watson−Crick base-pair. In addition, in the case of the pyr•pur-pyr motif, the Hoogsteen base-paired cytosine is protonated, leading to some charge

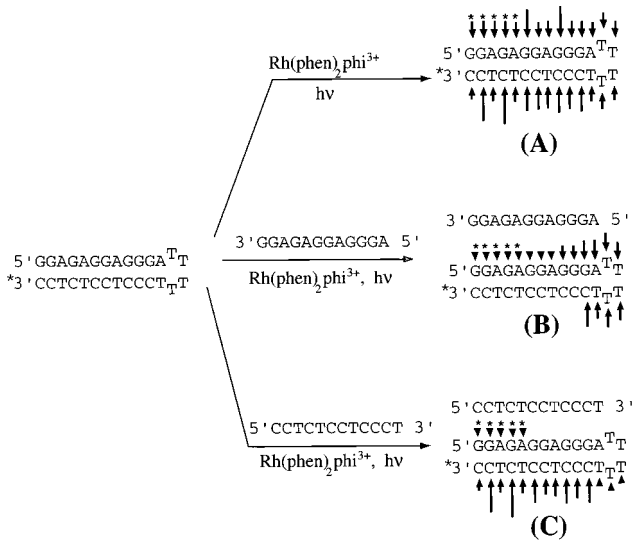

FIGURE 7: Schematic of $Rh(phen)_2phi^{3+}$ cleavage on the DNA duplex (**A**), DNA pur•pur-pyr triplex (**B**), and DNA pyr•pur-pyr triplex (**C**). Relative cleavage intensities (as determined by integration using ImageQuant) are depicted by the size of the arrows. Arrows with asterisks are approximations only. Cleavage is evident throughout the duplex strand alone, while cleavage is seen on the purine side of the Watson−Crick duplex on the pur•pur-pyr motif. Cleavage is seen on the pyrimidine side of the Watson−Crick duplex on the pyr•pur-pyr motif.

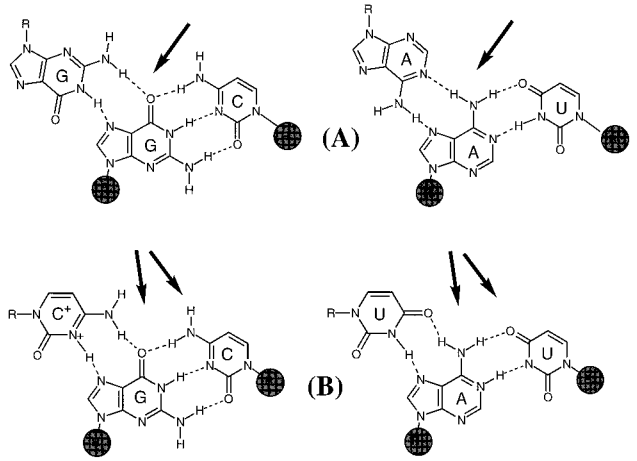

FIGURE 8: Schematic of cleavage by $Rh(phen)_2phi^{3+}$ of the pur•pur-pyr motif (**A**) and the pyr•pur-pyr motif (**B**). Stippled sugars show the nucleotides cleaved. Arrows show the probable direction of intercalation of the phi ligand.

repulsion with the positively charged metal complex. To a first approximation, therefore, cleavage could be distributed fairly evenly on the Watson−Crick pair, but not on the Hoogsteen strand. It is noteworthy in this context that cleavage results from a hydrogen abstraction reaction by the phi with the ribose, not with the nucleic acid base. Nonetheless, molecular modeling on a triple helix, assuming all bases to be in the anti configuration, reveals in three dimensions that access to the sugar correlates directly with the orientation on the base stack.

One observation with respect to the RNA triple helix which emerges from these studies involves the conformational change apparent in the hairpin loop upon triplex formation. Although the tetrauridine hairpin loop of the RNA duplex is not cleaved by the metal complex, addition of either third strand, with resultant triple helix formation, leads to a structural change in the loop which renders the loop hypersensitive to the metal complex. Earlier studies with $Rh(phen)_2phi^{3+}$ have suggested that only tightly stacked or structured loops are targeted by the metal complex (*3*). The hypersensitivity observed may then point to a helical unwinding that accompanies the formation of the triple helix. Such unwinding would generate a torque in the neighboring loop and alter how the bases are packed within the loop, rendering the tighter stacking a preferred target for the rhodium intercalator. It seems unlikely that electrostatics play a major part in this hypersensitivity given the complete absence of reaction within the duplex loop, where the electrostatic considerations are equivalent. Clear changes are also detected by probing with RNases where in a complementary experiment, the loop region of the duplex when the third strand is bound to form the triplex is found to be less susceptible to RNase digestion than is the loop in the duplex alone. It is worth noting that the rhodium complex promotes a hypersensitive reaction in the loop region of the DNA triple helices as well, although the conformational change associated with forming a triple helix from a B-form versus A-form duplex is clearly different.

This suggests a structural resemblance between the two triplex forms. The pattern of cleavage across the triplex does differ between the two motifs, but this difference may result from a difference in how the metal complex is oriented in the helical stack rather than a structural difference between the triple helices (vide supra). It is difficult to make a comparison of the photoreactions of either motif at pH 5.5 because the pyr•pur-pyr motif is formed in lower yield than the pur•pur-pyr motif even at that pH. Without accounting for the lower yield of formation of the pyr•pur-pyr helix, it appears that the pyr•pur-pyr motif is cleaved less than half as efficiently as the pur•pur-pyr motif, based on phosphorimager quantitation. Comparisons between RNA and DNA triple helices are more difficult to make because of the inherently strong reactivity of the metal complex with the B-form duplex alone.

Rh(phen)$_2$phi^{3+} as a Probe of Naturally Folded RNAs. Our results on the synthetic triple helices provide a strong foundation for understanding the cleavage patterns already obtained on different tRNAs as well as for new mapping studies on folded RNAs. For example, $tRNA^{Phe}$ contains a central triple base interaction, m^7G46-G22-C13 (*16*), and strong cleavage is observed by $Rh(phen)_2phi^{3+}$ at G22 and m^7G46, and with none at C13. This cleavage pattern is fully consistent with the results on the pur•pur-pyr synthetic triplex, as cleavage is seen on the purine strand of the duplex, even though the triplex does not contain the methylated G. Interestingly, when G46 is mutated to a C, cleavage at C46 is lost (*3*), while with the mutation G46A-G22A-C13U, which preserves the pur•pur-pyr triplex motif, cleavage is maintained. In the case of the analogous triple A46•G22-Ψ13 on $tRNA^{Asp}$, cleavage is centered on the Hoogsteen purine•purine base-pair. Again, this is consistent with the cleavage seen on the pur•pur-pyr synthetic triplex. Thus generally, results obtained on the tRNAs may be understood in the context of the synthetic triple helices.

These studies therefore lay the groundwork for probing folded RNAs which have not yet been structurally characterized in sufficient detail. $Rh(phen)_2phi^{3+}$ serves as a chemical probe to delineate positions where nucleotides form triply

bonded arrays, though, of course, some such arrays in the interior of larger folded RNAs would not be accessible. Nonetheless, $Rh(phen)_2phi^{3+}$ is expected to cleave at selective sites on a folded RNA which are not part of an A-form duplex. Instead, these sites would represent those in which the major groove is made accessible to intercalative stacking, either through a bulged or mismatched opening which disrupts the A-form duplex or through a tertiary interaction involving a triply bonded array. In concert with mutational studies, then, the application of $Rh(phen)_2phi^{3+}$ to probe RNA now represents a valuable strategy to delineate RNA tertiary structure.

ACKNOWLEDGMENT

We thank E. Theil for helpful suggestions during the course of this research.

REFERENCES

1. Chow, C. S., and Barton, J. K. (1990) *J. Am. Chem. Soc. 112*, 2839−2841.
2. Chow, C. S., Hartmann, K. M., Rawlings, S. L., Huber, P. W., and Barton, J. K. (1992) *Biochemistry 31*, 3534−3542.
3. Chow, C. S., Behlen, L. S., Uhlenbeck, O. C., and Barton, J. K. (1992) *Biochemistry 31*, 972−982.
4. Chow, C. S., and Bogdan, F. M. (1997) *Chem. Rev. 97*, 1489−1513.
5. Burrows, C. J., and Rokita, S. E. (1994) *Acc. Chem. Res. 27*, 295−301.
6. Felsenfeld, G., Davies, D. R., and Rich, A. (1957) *J. Am. Chem. Soc. 107*, 5528−5529.
7. Strobel, S. A., Moser, H. E., and Dervan, P. B. (1988) *J. Am. Chem. Soc. 110*, 7927−7929.
8. Moser, H. E., and Dervan, P. B. (1987) *Science 238*, 645−650.
9. Beal, P., and Dervan, P. B. (1991) *Science 251*, 1360.
10. Broitman, S. L., Im, D. D., and Fresco, J. R. (1987) *Proc. Natl. Acad. Sci. U.S.A. 84*, 5120−5124.
11. Chastain, M., and Tinoco, I., Jr. (1992) *Nucleic Acids Res. 20*, 315−318.
12. Letai, A. G., Palladino, M. A., Fromm, E., Rizzo, V., and Fresco, J. R. (1988) *Biochemistry 7*, 9108−9112.
13. Mirkin, S. M., Lyamichev, V. I., Drushlyak, K. N., Dobrynin, V. N., Filipov, S. A., and Frank-Kamenetskii, M. D. (1987) *Nature 330*, 495−497.
14. de los Santos, C., and Rosen, P. (1989) *Biochemistry 28*, 7282−7289.
15. Vlieghe, D., Vanmeervelt, L., Dautant, A., Gallois, B., Precigoux, G., and Kennard, O. (1996) *Science 273*, 1702−1705.
16. Kim, S.-H., Sussman, J. L., Suddath, F. L., Quigley, G. J., McPherson, A., Wang, A. H., Seeman, N. C., and Rich, A. (1974) *Proc. Natl. Acad. Sci. U.S.A. 71*, 4970−4974.
17. Quigley, G. J., and Rich, A. (1976) *Science 194*, 796−806.
18. Cate, J. H., Gooding, A. R., Podell, E., Zhou, K. H., Golden, B. L., Kundrot, C. E., Cech, T. R., and Doudna, J. A. (1996) *Science 273*, 1678−1685.
19. David, S. S., and Barton, J. K. (1993) *J. Am. Chem. Soc. 115*, 2984−2985.
20. Pyle, A. M., Long, E. C., and Barton, J. K. (1989) *J. Am. Chem. Soc. 111*, 4520−4522.
21. Sitlani, A., Long, E. C., Pyle, A. M., and Barton, J. K. (1992) *J. Am. Chem. Soc. 114*, 2303−2312.
22. Hudson, B. P., Dupureur, C. M., and Barton, J. K. (1995) *J. Am. Chem. Soc. 117*, 9379−9380.
23. Campisi, D., Morii, T., and Barton, J. K. (1994) *Biochemistry 33*, 4130−4139.
24. Mergny, J.-L., Duval-Valentin, G., Nguyen, C. H., Perroualt, L., Faucon, B., Rougée, M., Montenay-Garestier, T., Bisagni, E., and Hélène, C. (1992) *Science 256*, 1681−1684.
25. Scaria, P. V., and Shafer, R. H. (1991) *J. Biol. Chem. 266*, 5417−5423.
26. Tuite, E., and Norden, B. (1995) *Bioorg. Med. Chem. 3*, 701−711.
27. Jenkins, Y., Friedman, A. E., Turro, N. J., and Barton, J. K. (1992) *Biochemistry 31*, 10809−10816.
28. Marchand, C., Bailly, C., Nguyen, C. H., Bisagni, E., Garestier, T., Hélène, C., and Waring, M. J. (1996) *Biochemistry 35*, 5022−5032.
29. Lee, J. S., Latimer, L. J. P., and Hampel, K. J. (1993) *Biochemistry 32*, 5591−5597.
30. Pilch, D. S., Kirolos, M. A., and Breslaur, K. J. (1995) *Biochemistry 34*, 16107−16124.
31. Kane, S. A., Hecht, S. M., Sun, J. S., Garestier, T., and Helene, C. (1995) *Biochemistry 34*, 16715−16724.
32. Lim, A. C., and Barton, J. K. (1993) *Biochemistry 32*, 11029−11034.
33. Weeks, K. M., and Crothers, D. M. (1993) *Science 261*, 1574−1577.
34. Roberts, R. W., and Crothers, D. M. (1991) *Proc. Natl. Acad. Sci. U.S.A. 88*, 9397−9402.
35. Roberts, R. W., and Crothers, D. M. (1992) *Science 258*, 1463−1466.
36. England, T. E., and Uhlenbeck, O. C. (1978) *Nature 275*, 560−561.
37. Peattie, D. A. (1979) *Proc. Natl. Acad. Sci. U.S.A. 76*, 1760.
38. Sambrook, J., Fritsch, E. F., and Manniatis, T. (1989) *Molecular Cloning*: *A Laboratory Manual*, 2nd ed., Cold Spring Harbor Laboratory Press, Cold Spring Harbor, NY.
39. Semerad, C. L., and Maher, L. J. (1994) *Nucleic Acids Res. 22*, 5321−5325.
40. Krotz, A. H., Kuo, L. Y., and Barton, J. K. (1993) *Inorg. Chem. 32*, 5963−5974.
41. Singleton, S. F., and Dervan, P. B. (1992) *Biochemistry 31*, 10995−11003.
42. Chow, C. S. Ph.D. Thesis. California Institute of Technology, Pasadena, CA, 1991.
43. Plu, G. E., Park, Y.-W., Singleton, S. F., Dervan, P. B., and Breslauer, K. J. (1990) *Proc. Natl. Acad. Sci. U.S.A. 87*, 9436−9440.
44. Kuchino, Y., and Nishimura, S. (1989) *Methods Enzymol. 180*, 154−163.

BI980509V